Exploring Cosmic Evolution with the FORS Deep Field

The FORS instruments at the ESO VLT have been used to study the cosmic evolution of galaxies. From a large sample of distant galaxies observed near the South Galactic Pole we obtained new results on the physical properties of high-redshift galaxies, on the evolution of the galaxy luminosity function and of the cosmic star formation rate, on the chemical enrichment of the universe, and other signposts for changes with cosmic time.

I. Appenzeller[1],
R. Bender[2,5], A. Böhm[3],
S. Frank[4], K. Fricke[3],
A. Gabasch[2], J. Heidt[1],
U. Hopp[2], K. Jäger[3],
D. Mehlert[1], S. Noll[1],
R. Saglia[5], S. Seitz[2],
Ch. Tapken[1],
B. Ziegler[3]

[1]Landessternwarte, Heidelberg, Germany
[2]Universitäts-Sternwarte München, Germany
[3]Universitäts-Sternwarte Göttingen, Germany
[4]Ohio State University, Columbus, Ohio, USA
[5]MPE, Garching, Germany

The idea of a "FORS Deep Field" (FDF) was born in 1997 when scientists at the Heidelberg State Observatory and the University Observatories of Göttingen and München drew up plans for the use of the guaranteed observing time granted to them as a reward for building the two FORS instruments for the ESO VLT. By that time various deep field projects (notably the HDF-N) had already resulted in important new information on the distant universe and its evolution with cosmic age. But the combination of the larger (relative to the HDF) field-of-view of FORS, the excellent optical quality of the VLT, and the superior light collecting power of the VLT combined with the high efficiency of the FORS spectroscopic observing modes promised important new opportunities in this area. Therefore, a significant fraction of the guaranteed FORS observing time was set aside for very deep observations of a carefully selected region of the southern sky corresponding to the field-of-view of FORS in standard resolution mode. A description of the selection criteria, of the objectives of the FDF programme, and of various technical details has been provided in an earlier issue of *The Messenger* (Appenzeller et al., 2000), and thus will not be repeated here. Instead, the present contribution will be devoted to highlights among the scientific results obtained so far from the FDF.

Observing a complete sample of distant galaxies

The FDF programme started in 1999 as soon as the first unit telescope of the VLT became available for scientific work. As a first step we used FORS1 at the VLT unit telescope Antu to obtain deep images of the FDF through five standard broad-band filters (*U, B, g, R*, and *I*) during 1999 and 2000. The broad-band images were later supplemented with narrow-band images taken through selected interference filters. Although observing conditions during the 1999 runs were rather unfavourable and part of the time was lost to poor weather, it was eventually possible to collect more than 300 individual images with a total integration time of about 39 hours. The resulting co-added FORS image for the blue filter band turned out to be nearly as deep as the corresponding HDF-N image, while the visual and the *I*-band images were only about one magnitude less deep than those of the HDF-N. Of course, due to the atmospheric blurring typical of ground-based observations, the FORS images are less sharp than those of the HST deep fields. On the other hand, with (FWHM) angular resolutions ranging between 0.53 arcsec in the *I* and 0.97 arcsec in *U*-band, the resolution of the FDF images compares favourably with other ground-based deep fields. As a result, on our images, which cover a sky area of about seven by seven arcmin (or 1/15 of the area covered by the full moon), more than 10 000 objects are visible, i.e. the same number of objects as in the new (much deeper, but smaller) "HST Ultra Deep Field". Almost all objects are distant galaxies. There are also eight spectroscopically confirmed quasars and more than 50 faint stars. A colour image of the FDF, produced by combining our *B* (blue), *R* (red) and *I* (deep red) monochromatic images is presented in Fig. 1. To make fine details and the fainter objects better visible, an image sharpening procedure (the Lucy-Richardson deconvolution algorithm) and a non-linear flux scale has been applied to the original image. Therefore the image has an effective resolution of about 0.4 arcsec, but a somewhat higher noise level than the original images.

In addition to the FORS frames we obtained near-infrared (*J* and *Ks* bands) images of the FDF using the SofI instrument at the ESO NTT on La Silla. Due to the smaller telescope aperture, these images are much less deep. But they were important for the analysis of our data as they improved the accuracy of the photometric redshifts and they helped us to discriminate between very

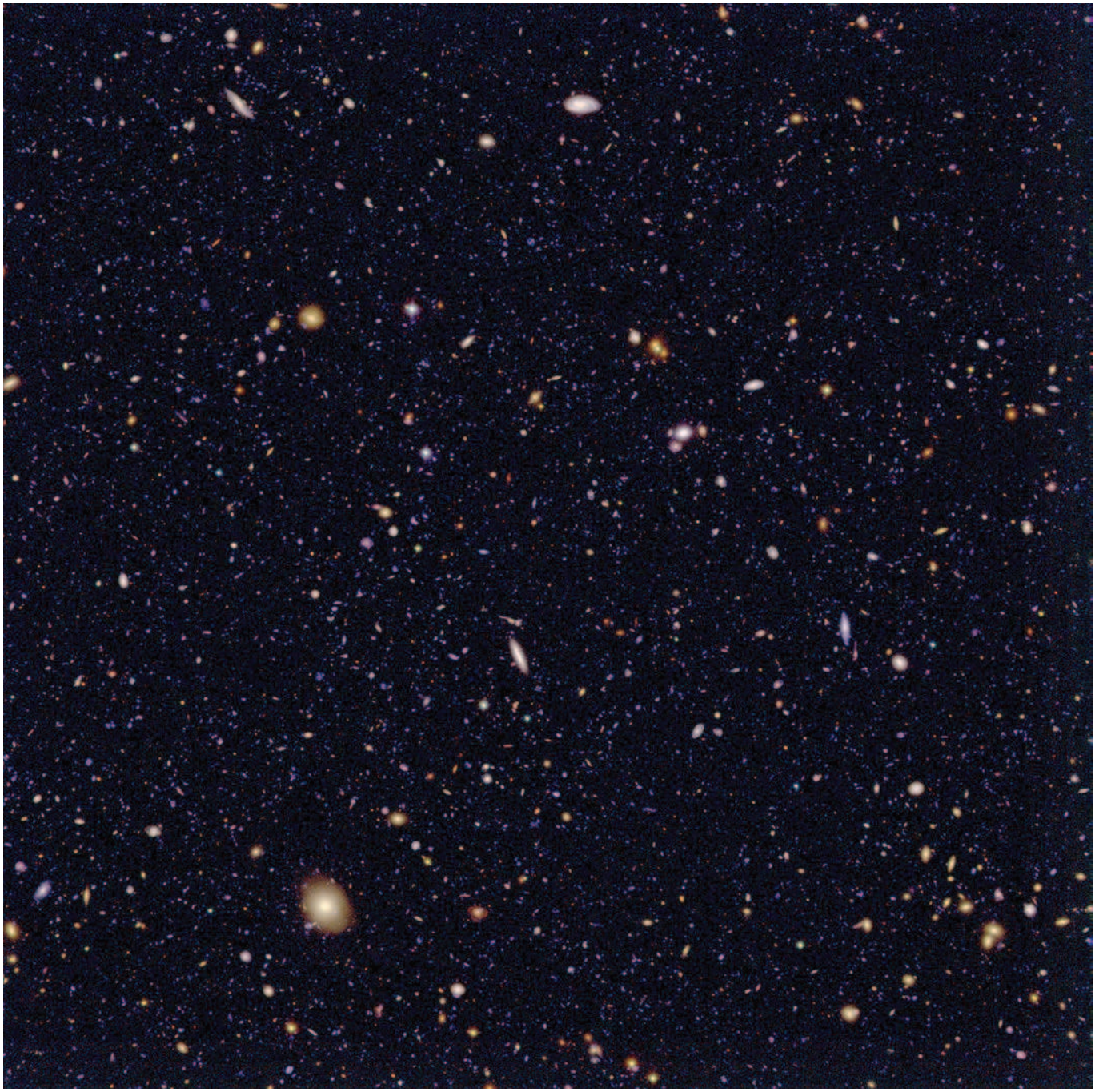

Figure 1: Colour image of the FORS Deep Field. The image was produced by combining images obtained in a blue, a red and a deep-red filter band. As pointed out in the text it has been processed to increase the resolution (to about 0.4 arcsec) and to make fainter features visible. The image covers a field of 7.1 × 7.1 arcmin^2. North is up, east to the left.

red compact galaxies and very cool stars. The large number of distant galaxies and the uniform conditions under which the different images were obtained make the FDF survey a unique data base for studying extragalactic stellar systems at different distances and cosmic ages. However, to evaluate our images, first the flux recorded from the individual objects had to be measured accurately. With about 10^4 targets this obviously required automatic procedures. While such procedures are standard tools of modern astronomy, their application to the FDF images turned out to be more complex than expected. Part of the difficulties encountered were due to the fact that most of our objects had (even in the moonless nights used for this programme) a surface brightness amounting to only a small fraction of the brightness of the night sky. Hence the background and the instrumental response functions had to be determined with very high accuracy to avoid introducing errors from an incorrect background subtraction. Moreover, instrumental effects and unresolved faint background galaxies produced unusual noise properties and artifacts which had to be studied and taken care of. As a result it took about two years of hard work to produce a catalogue of all objects for which the brightness could be measured with an error at least five times smaller than the observed value. This catalogue, published by Heidt et al. (2003), lists the coordinates, the brightness in the different filter bands, and other properties of 8753 FDF objects.

The redshift distribution of the FDF Galaxies

Because of the expansion of the universe, the wavelength of the light which we receive from distant galaxies is always shifted to a value larger than the wavelength at which the light had been emitted. Today astronomers normally describe this 'red-

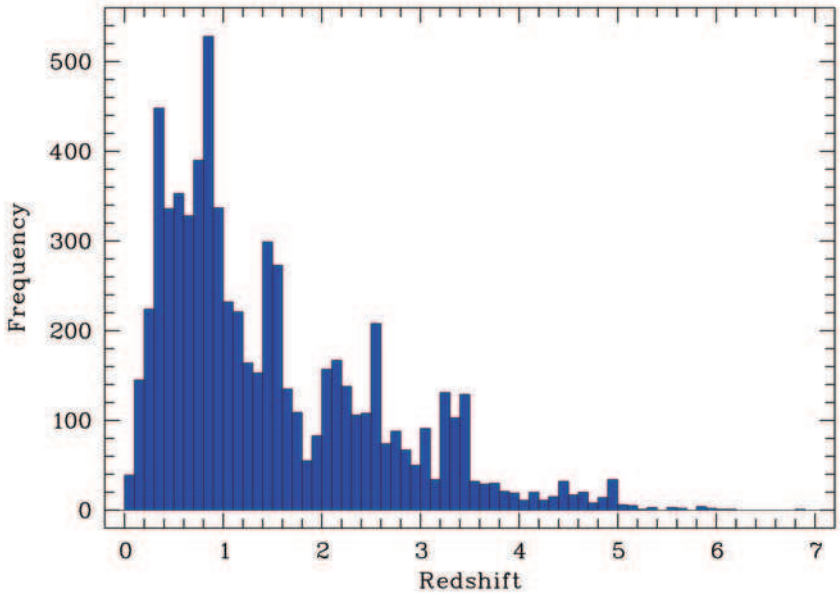

Figure 2: The distribution of the photometric redshifts in the FDF. The ordinate gives the number of galaxies observed within redshift intervals of 0.1.

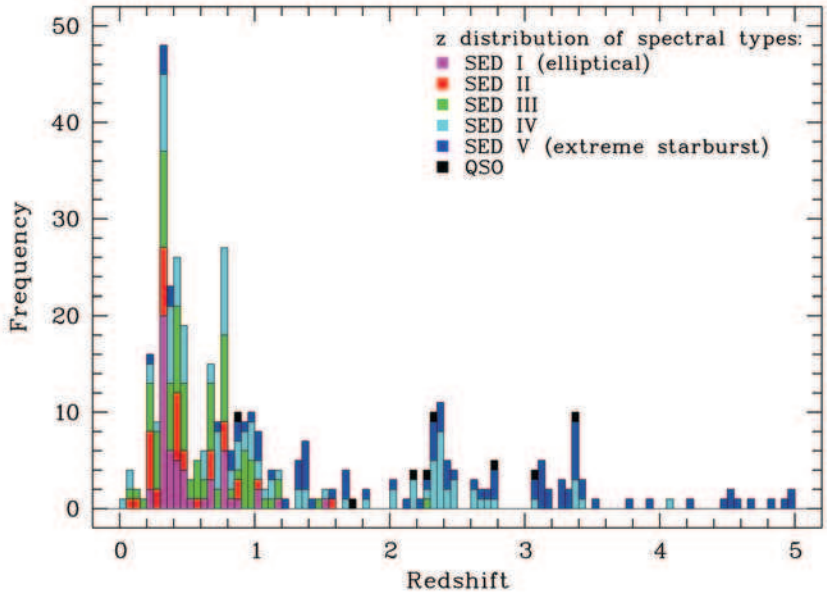

Figure 3: The distribution of the well measured spectroscopic redshifts in the FDF. The ordinate gives the number of galaxies per redshift interval of 0.05. The colours differentiate galaxies with different levels of star formation activity, ranging from insignificant star formation (magenta) to extreme starbursts (dark blue).

shift' by a dimensionless quantity denoted as z which is the ratio between this wavelength shift and the wavelength at which the light was emitted. Since the spectra of galaxies contain spectral lines and continuum features with known emitted wavelengths, redshifts can be derived from spectra or – less accurately – from photometric data (as described for the FDF sample by Bender et al. 2001). Since the redshift increases with distance, it can be used to determine distances. Moreover, because of the finite velocity of light, redshifts also provide information on the epoch when the light was emitted. Hence, observing galaxies with high redshifts allow us not only to look into the distant universe but, more importantly, it allows us to look back into cosmic history. So far photometric redshifts have been derived for about 7000 FDF galaxies. But accurate spectroscopic redshifts (which take much more observing time) have been determined and catalogued for a subsample of 341 FDF objects only (Noll et al. 2004). For statistical investigations the larger data base of the photometric redshifts is obviously an advantage. On the other hand, these redshifts are less accurate than those derived from spectra. Fortunately, for those FDF objects where both types of redshifts have been derived, a comparison has shown that the average mean error of our photometric redshifts is only about 0.03 for small redshifts (increasing proportional to $(1+z)$ for larger z), which is sufficient for most statistical purposes.

In Figs. 2 and 3 we present the distributions of the observed photometric and spectroscopic redshifts. As shown by Fig. 2 the number of observed galaxies increases rapidly with redshift for $z < 0.5$ and decreases again gradually for $z > 1$. As has been known from earlier studies, the initial increase reflects the increasing volume of space sampled with increasing redshift, while the decrease is due to the fact that at high redshifts (i.e. at large distances) we observe only the rare luminous galaxies. The range of redshifts in Fig. 2 ($0 < z < 7$) corresponds to a distance range of 0–13 billion light years or a look-back time of up to 13 billon years (which covers more than 90% of the present age of the universe). The appearance of FDF galaxies of different redshifts is illustrated by Fig. 4. As shown by this figure, at intermediate redshifts many galaxies appear blue due to the redshifted UV-radiation of massive young stars. At very high redshifts galaxies appear deep red and rather compact.

While Fig. 2 provides an essentially correct representation of the redshift distribution of our flux-limited FDF galaxy sample, Fig. 3 is affected by selection effects. Firstly, in order to include a sufficient numbers of distant galaxies, during the spectroscopic observations priority was given to targets with higher photometric redshifts. Therefore, compared to Fig. 2 our Fig. 3 contains a larger fraction of high-redshift objects. Secondly, galaxies with redshifts around $z = 1.5$ have no strong spectral features in the wavelength range accessible with FORS. Hence, although many such objects were observed, accurate redshifts could often not be determined, resulting in a dearth of such galaxies in Fig. 3. Our data also show that at different redshifts different types of galaxies tend to be observed. Typical elliptical galaxies, containing no young blue stars, are observed at low redshift only (since at higher redshifts their radiation is shifted out of the wavelength range of FORS). On the other hand, star forming galaxies can be observed at any redshift (≤ 7).

A characteristic property of Figs. 2 and 3 are conspicuous maxima of the galaxy densities at distinct redshifts (e.g. at $z = 0.3$, 0.8, 2.4, and 3.4). Because of the lower accuracy of the photometric redshifts, these maxima appear broader in Fig. 2. But they are present in both (independently derived) distributions and they obviously reflect the sponge-like large-scale structure of the matter distri-

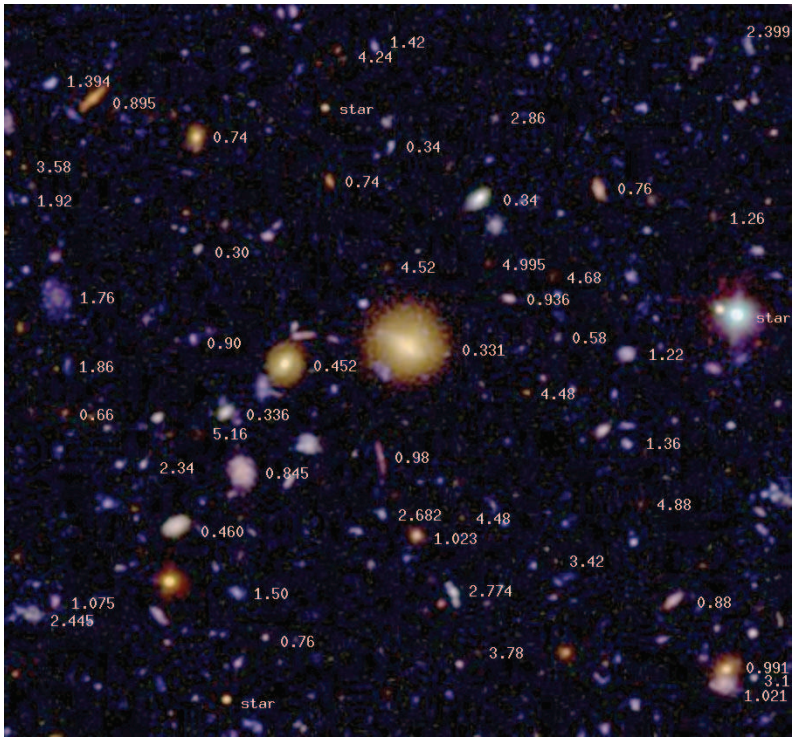

Figure 4: The appearance of FDF galaxies of different redshift. Examples of the observed redshifts are indicated by numbers placed to the right of the corresponding object. Three decimals indicate spectroscopic redshifts, 2 decimals photometric redshifts. The image covers about 80″ by 90″. North is up, east to the left. The bright (yellowish) elliptical galaxy near the centre (with z = 0.331) is FDF-6005. It is one of the brightest FDF galaxies and one of the few FDF objects visible on the Palomar Observatory Sky Survey. The galaxy north-west of FDF-6005 with z = 4.995 is one of the most distant FDF objects for which a spectroscopic redshift has been derived so far.

bution in the universe. A detailed analysis shows that the observed structure agrees well with the predictions of the CDM scenarios of cosmic structure formation. The conspicuous overdensity of galaxies at $z \approx 0.3$ can be traced to a galaxy cluster which is directly visible in the lower right of Fig. 1.

Observing cosmic evolution

Among the important new results of the FDF programme are new insights into the evolution with cosmic time of the properties of galaxies. Since our photometric redshift sample contains galaxies with very different redshifts and (at all redshifts) of very different intrinsic luminosity, it is particularly well suited to derive the luminosity distribution of galaxies as a function of the redshift (and cosmic age). Therefore, as described in detail by Gabasch et al. (2004), we were able to derive luminosity distributions for the FDF galaxies up to redshifts of 5, i.e. for about 90% of the cosmic history. Out to a redshift of 2.5, the UV data can be described with a flat slope of the luminosity function not changing throughout time ($\alpha = -1.1$ in the Schechter notation). The slope in the rest frame blue is slightly steeper and also constant with time. At even higher redshifts, we found no evidence for the very steep slopes ($\alpha = -1.6$) discussed for Lyman break galaxies in the literature. The analysis of the luminosity function fits between 0.5 and 5 yields a brightening of the UV rest frame characteristic magnitude by 2.6 mag and at the same time a decrease of the characteristic density by a factor of ten. The rest-frame luminosity functions furthermore allow us to derive the star formation rates as a function of cosmic time or redshift. From earlier investigations it has been known that, compared to today, star formation occurred at a much higher rate during the first few billion years of the cosmic history. As illustrated by Fig. 5 the FDF data confirm this result. Furthermore, the FDF results favour a scheme of the galaxy evolution where the overall star formation have stayed almost constant up to very early ages of the universe. Even more direct evidence for a change of the properties of the star forming galaxies with cosmic age is shown in Fig. 6. This figure (from Noll et al. 2004) compares the average spectra of FDF starburst galaxies observed in the redshift range $3 < z < 4$ (corresponding to a cosmic period when the universe had reached about 10% to 15% of its present age) and $2 < z < 3$ (corresponding to the time when the universe had reached about 15% to 25% of its present age). As shown by the figure, the spectra show the same basic features, but distinct quantitative differences. As an example we note that the galaxies observed at the earlier cosmic epochs show on average much stronger Ly-α emission and weaker absorption lines of heavy elements. Moreover, the UV continuum appears steeper. As pointed out by Noll et al. (2004) these differences can be explained assuming a lower abundance of heavy elements and a lower average mass of the star forming galaxies at the earlier epoch. This is not unexpected since we know that during the Big Bang only hydrogen and helium nuclei had been formed while practically all other elements were produced later in stars. In the FDF we obviously look back into epochs where the universe was too young to have already formed the fraction of heavy elements which we observe today.

A more quantitative view of the chemi-

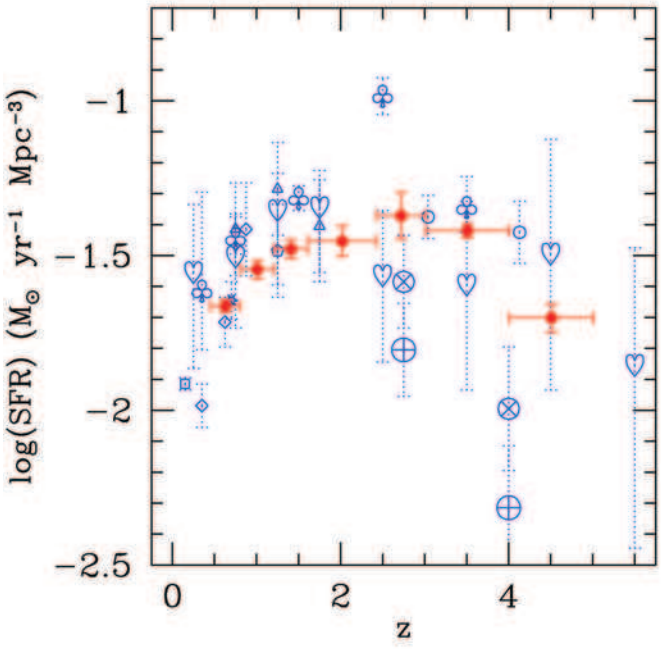

Figure 5: The cosmic star formation rate as a function of redshift as derived from the FDF (red symbols). For comparison we also included the results of various earlier studies taken from the literature (blue symbols). The data have not been corrected for dust extinction.

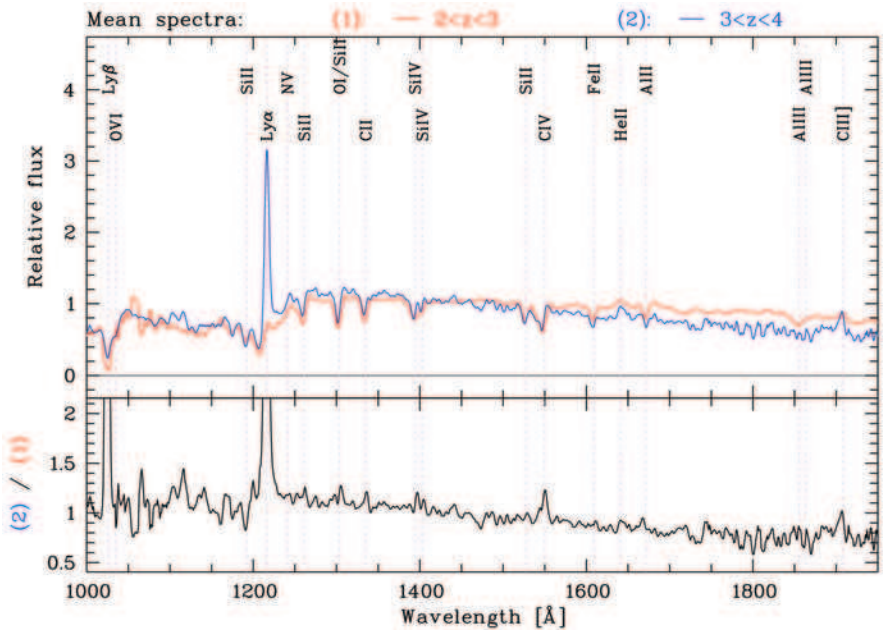

Figure 6: Comparison of the mean spectra of FDF starburst galaxies with redshifts $2 < z < 3$ (red solid line) and $3 < z < 4$ (blue solid line). The spectra are normalized to have the same flux level at the (rest frame) wavelength 1425 Å. The lower panel shows the ratio between the two spectra.

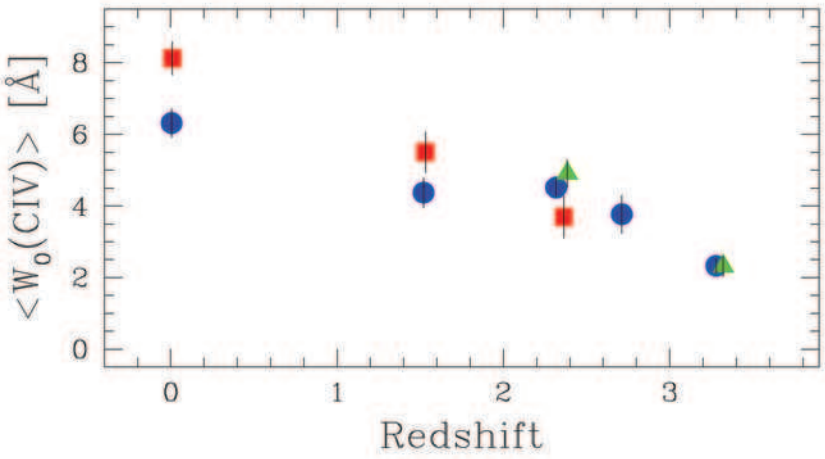

Figure 7: Mean strength of the resonance doublet of the carbon ion C^{+++} in the spectra of FDF starburst galaxies as a function of redshift. Since in starburst galaxies the strength of this blend is approximately proportional to the abundance of heavy elements, the diagram illustrates directly the chemical enrichment of the universe with decreasing redshift (or increasing cosmic age).

cal enrichment of the universe by stars is provided by Fig. 7 (from Mehlert et al. 2002) where the strength (in terms of the rest-frame equivalent width W_0) of the resonance doublet of the carbon ion C^{+++} in the spectra of starburst galaxies is plotted as a function of the redshift. The data points at $z > 1$ are from the FDF. The point at $z = 0$ is based on published spectra of local starburst galaxies. The blue symbols include all galaxies for which the line was measured. The green and red symbols refer to luminosity-selected subsamples which were investigated separately to make sure that the observed variation is not due to a selection effect. (For details see Mehlert et al., 2002). Since in local starburst galaxies the C^{+++} strength is found to be approximately proportional to the heavy element content, the blue data points in Fig. 7 trace directly the chemical enrichment history of the universe. According to this figure about 2/3 of the heavy nuclei seem to have been formed already at $z \approx 2.5$, i.e. during the first few billion years of the cosmic history. This result is in good agreement with the high star formation activity at these early epochs indicated by Fig. 5.

The Tully-Fisher relation at intermediate redshifts

Evolutionary effects such as those described above may also affect established relations between different properties of galaxies, such as the Tully–Fisher relation (TFR, Tully & Fisher 1977) connecting the luminosity and the maximum rotation velocity of the discs of spiral galaxies. This relation can be understood as a combination of the virial theorem and the centrifugal support of spiral galaxies. Comparing the TFR of present-day spirals and that of distant galaxies observed at earlier cosmic epochs, it is possible to quantify the evolution in luminosity which the spirals have undergone. This makes the TFR a powerful tool to test predictions of numerical simulations based on the hierarchical scenario of galaxy formation, according to which small galaxies have formed first, followed by the successive build-up of larger systems via merging processes. However, observational studies of the TFR of distant galaxies were so far limited to small samples with 10–20 objects and thus could not be used to test whether the luminosity evolution differs between slowly rotating (i.e. low-mass) and rapidly rotating (high-mass) spirals. Therefore, we carried out medium–resolution spectroscopy of 113 FDF spiral galaxies covering redshifts between $z = 0.1$ and $z = 1$ (Ziegler et al. 2002, Böhm et al. 2004).

From these spectra we extracted spatially resolved rotation curves. By fitting simulated velocity fields to the observed rotation curves, the maximum rotation velocity could be derived for 77 FDF spirals. The simulations took into account all geometric effects and, in particular, the seeing and the influence of the slit width. In Fig. 8, we compare our sample to the local TFR. The FDF sample was sub-divided according to the rotation curve quality. Solid symbols in Fig. 8 denote high-quality rotation curves with a large spatial extent and high symmetry, which yield robust values of the maximum rotation velocity. While the distant low-mass spirals were found to be brighter by up to 2 magnitudes in the rest–frame *B*-band than their local counterparts, the high-mass objects do not show a significant evolution in luminosity. This offers an explanation for the discrepancies between previous studies of the distant TFR as combination of selection effects and small number statistics. Our finding is at variance with the results of numerical simulations, which predict a stronger brightening of *high-mass* spirals. This may indicate the need for a more realistic modeling of the stellar population properties in *N*-body codes.

Ly-α galaxies

In addition to results of a statistical nature, the FDF also yielded new information on individual objects and on interesting particular classes of objects. Examples are the so-called "Ly-α galaxies". These are starburst galaxies showing extremely strong Ly-α emission lines relative to the continuum. Such objects are not observed in the local universe but (as also indicated in Fig. 6) they become rather common at high redshifts.

Their strong Ly-α flux is surprising since multiple resonance scattering in this line results in a very long effective light path of this radiation. Hence any dust absorption will reduce the escape probability of Ly-α photons dramatically. Therefore, it has been suggested in the literature that the high-redshift Ly-α galaxies are very young galaxies which do not yet contain heavy elements which could condensate into dust particles. However, our FORS spectra (e.g. Fig. 9) contain conspicuous spectral lines of carbon, silicon and nitrogen, showing that such objects are not devoid of heavy elements. In fact, a model fit of the spectrum of the z = 3.304 Ly-α galaxy FDF-4691 indicates for this object a heavy element abundance comparable to that of the Magellanic Clouds (the closest major companion galaxies of the Milky Way; Tapken et al., 2004). Hence Ly-α photons obviously escape from this galaxy in spite of the presence of heavy elements, i.e. in the presence of matter which can form dust. A detailed model comparison and dedicated radiative transfer calculations for FDF-4691 have shown that this is possible since the Ly-α line is formed in a highly turbulent medium and since the line-of-sight HI column density is relatively low.

Galaxies and the Intergalactic Gas

Among the eight quasars in the FDF one (Q0103-260, z = 3.36) is sufficiently bright for high-resolution spectroscopy. Therefore, we used the UVES echelle spectrograph at the VLT to study the absorption by the intergalactic gas in the direction of the FDF (Frank et al., 2003). As expected we found a close correlation between the redshift distribution of the intergalactic absorbers and of the galaxy density along the line-of-sight. As illustrated by Fig. 10, this correlation is particularly evident for the "metal absorption systems" which trace the high-density intergalactic matter. Since according to current CDM structure formation scenarios galaxies form first and most efficiently in volumes of the highest dark matter density (which also are regions of high baryonic matter density) and since galactic winds are expected to enrich the intergalactic medium with heavy nuclei as soon as star formation and stellar evolution have set in, the observed correlation is not surprising. However, more interestingly, the correspondence of metal absorption and galaxy clustering is not complete and the metal line strengths vary significantly between the different systems. At z = 2.558 we find, e.g., a reliably identified close pair of metal absorption systems in an apparent void of galaxies. However, this may be due to the incompleteness of our spectroscopic survey at faint magnitudes. On the other hand, the existence of a prominent galaxy clustering at z = 2.34 without a detectable metal absorption system is unexpected. At this redshift metal systems are easily detected. Therefore, the absence of detectable metal absorption can only be explained assuming that (compared to the other galaxy clusterings) the galaxies at z = 2.34 have been less efficient in chemically enriching their environment.

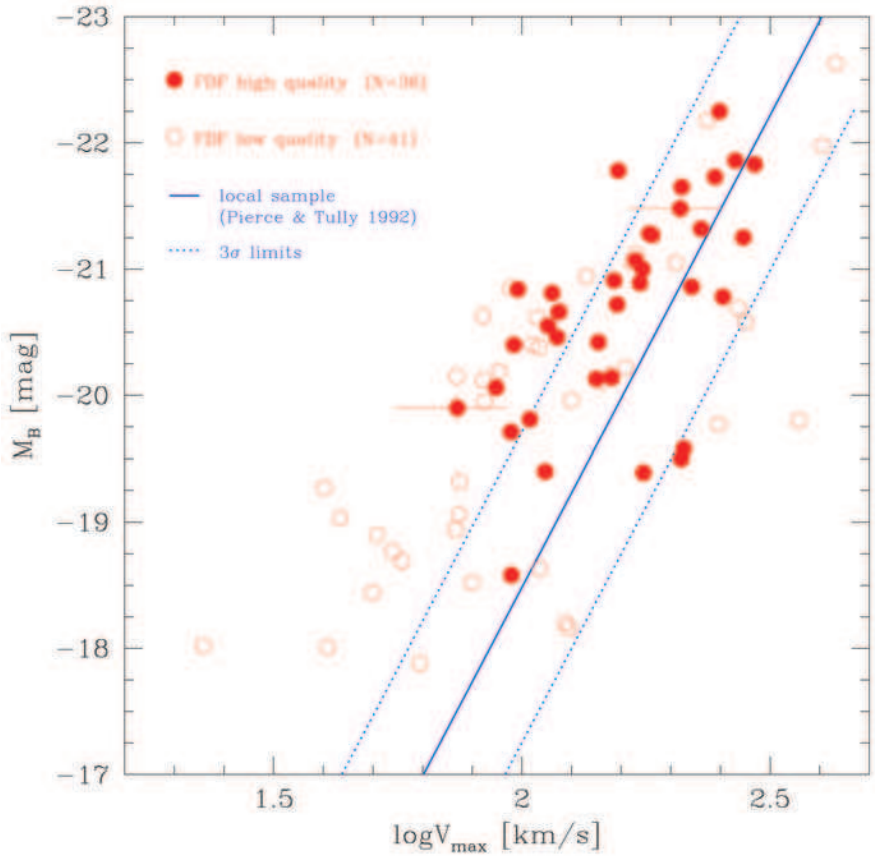

Figure 8: Blue absolute magnitudes M_B as a function of maximum disc rotation velocity V_{max} for 77 FDF spirals at redshifts 0.1 < z < 1.0 (red symbols), compared to the local Tully–Fisher relation (blue line). Slowly rotating, low–mass distant spirals are significantly brighter than their local counterparts, whereas distant and local high–mass systems have similar luminosities.

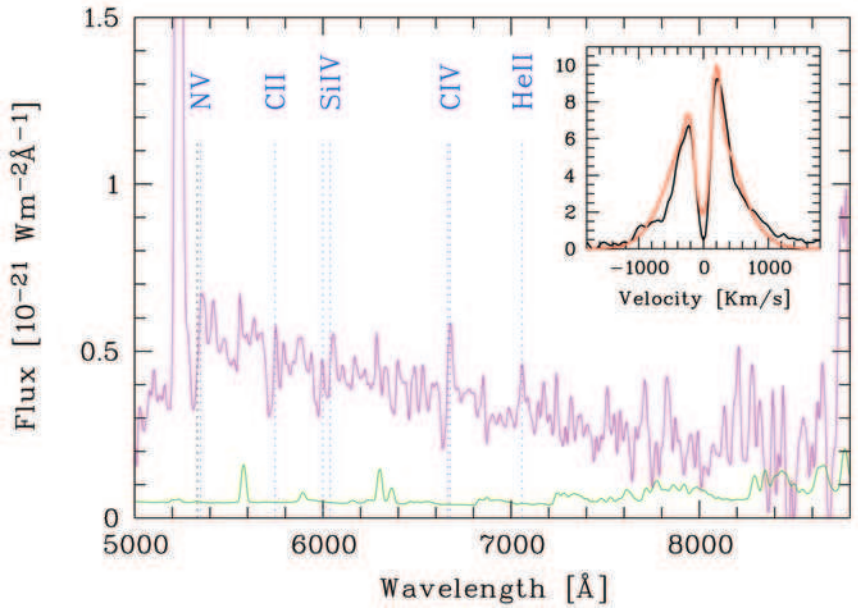

Figure 9: The spectrum of the Ly-α galaxy FDF-4691. In the low-resolution spectrum (magenta) the strong Ly-α line (observed at 5230 Å) is unresolved and truncated. The resolved profile of this line is presented in the inset (black line) together with a theoretical profile calculated from a model of the Ly-α forming region of FDF-4691 (red line).

With an angular size corresponding to the size of a large galaxy cluster at redshifts 2 - 5 the FDF is not well suited to study clustering effects in the angular distribution. On small scales, which can be investigated in the FDF, the observed clustering is consistent with the findings of other studies. But

there are a few regions which show an unexpected behavior. Most interesting is a surprisingly high density of galaxies with redshifts near 3.36 within a few arc sec (projected distance ≤ 60 kpc) of the bright QSO observed at this redshift. It may indicate that this QSO is located in an exceptionally dense protocluster at this redshift.

Ongoing and future work

In this report we described a few examples of scientific results obtained so far from the FDF. Many studies using FDF data are still in progress and some of the data (such as the stellar content of the FDF and observations obtained outside the optical range) have hardly been touched. Among the exciting ongoing investigations is a more thorough study of cosmic chemical evolution using medium resolution spectra of FDF galaxies (obtained with the VPH grisms of FORS2) and improved synthetic spectra. Moreover, a significant effort is being made to extend the FDF galaxy sample to redshifts $z > 5$. In this range different search techniques have to be used since such objects show no flux in most of the FORS broad-band filters (except for a weak signal at *I* in some cases). Using narrow-band observations in deep-red filter bands we were able to identify a sample of very promising candidates for such very high redshift galaxies in the FDF. However, these objects still require a spectroscopic confirmation. Hence there is still much work to be done in the FDF, and there remains a significant potential for more reports in *The Messenger.*

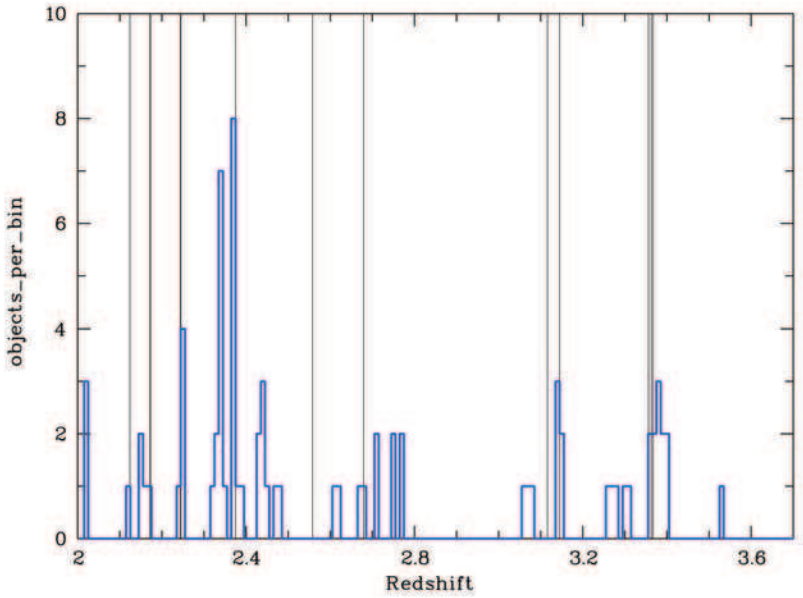

Figure 10: Histogram of the redshift distribution of spectroscopically observed FDF galaxies in the redshift interval $2 < z < 3.7$ (blue line) and the redshift positions of the metal absorption systems of the FDF quasar Q0103-260 observed in this redshift range (black vertical lines).

References

Appenzeller, I., et al., 2000, *The Messenger* **100**, 44
Bender, R., et al., 2001, Proc. ESO Conference on "Deep Fields", Springer 2001, p.96
Böhm, A., et al., 2004, A&A **420**, 97
Frank, S., et al., 2003, A&A **407**, 473
Gabasch, A., et al,: 2004, A&A **421**, 41
Heidt, J., et al., 2003, A&A **398**, 49
Mehlert, D., et al., 2002, A&A **393**, 809
Noll, S., et al., 2004, A&A **418**, 885
Tapken, C., et al., 2004, A&A **416**, L1
Tully, R.B., Fisher, J.R., 1977, A&A **54**, 661
Ziegler, B., et al., 2002, ApJ **564**, L69

Revisiting the orion Nebula

Wide Field Imager Provides New View of a Stellar Nursery (ESO PR Photo 20/04)

An international team of astronomers, led by Massimo Robberto (European Space Agency and Space Telescope Institute), used the Wide Field Imager (WFI), a 67-million pixel digital camera that is installed at the ESO/MPG 2.2m telescope at La Silla, to obtain very deep images of this region. The image shown is a false-colour composite of all of the images obtained in *B*, Hα, [OIII], and [SII] where each waveband was associated to a given colour: *B* to blue, [OIII] to green; Hα to orange, and [SII] to red. The field of view covers 34′ × 33′. North is up and East is to the left.
Among others, these observations allow the astronomers to measure the rates of mass that falls onto the young stars and to determine if it depends on the position of the stars in the cluster. If this were the case, it would indicate that the final stages of star formation are affected by the onset of ionizing radiation from the most massive stars. The astronomers also obtained images of the Orion Nebula in several narrow-band filters corresponding to emission lines - hydrogen (Hα), oxygen ([OIII]), and sulphur ([SII]) - enabling them to probe the morphology of the nebula in these prominent lines.